Chang Brian (Orcid ID: 0000-0001-5165-7051)

Title

Hybrid 3D-Printed Ear Tissue Scaffold with Autologous Cartilage Mitigates Soft Tissue Complications

Running title

Translatable hybrid 3D printed ear scaffold

Authors

Brian Chang MD, MS[1#], Ashley Cornett MS[2,3#], Zahra Nourmohammadi PhD[4], Jadan Law[5], Blaine Weld[5], Sarah J. Crotts MS[6], Scott J. Hollister PhD[6], Isabelle M.A. Lombaert PhD, MS[2,3], David A. Zopf MD, MS[5,7]

[#] Co-first authors

[1] Department of Pediatrics, UCLA Mattel Children's Hospital, 757 Westwood Plaza, Los Angeles, CA 90095, USA

[2] Department of Biologic and Materials Sciences, School of Dentistry, University of Michigan, 1011 N University, Ann Arbor, MI 48109, USA

[3] Biointerfaces Institute, University of Michigan, 2800 Plymouth Rd, Ann Arbor, MI 48109

[4] Department of Otolaryngology–Head and Neck Surgery, University of Michigan, 1540 E Hospital Dr., Ann Arbor, MI, 48109, USA

This is the author manuscript accepted for publication and has undergone full peer review but has not been through the copyediting, typesetting, pagination and proofreading process, which may lead to differences between this version and the Version of Record. Please cite this article as doi: 10.1002/lary.29114

[5] Department of Biomedical Engineering, Michigan Engineering, Ann & Robert H. Lurie Biomedical Engineering Building, 1101 Beal Ave., Ann Arbor, MI 48109, USA

[6] Center for 3D Medical Fabrication, Coulter Department of Biomedical Engineering, Georgia Institute of Technology, 313 Ferst Drive, Atlanta, GA, 30332, USA

[7] Department of Otolaryngology Head & Neck Surgery, Michigan Medicine, C.S. Mott Children's Hospital, 1540 East Hospital Drive, Ann Arbor, MI 48109, USA

Accepted as podium presentation at ASPO 2020 in Atlanta, GA, but conference was cancelled due to Covid pandemic. Re-submitted as ePoster.

Corresponding author

David Zopf, MD, MS

Department of Paediatric Otorhinolaryngology Head & Neck Surgery

CS Mott Children's Hospital

Michigan Medicine

1540 E Hospital Drive, SPC 4241

Ann Arbor, MI 48109-4241

United States of America

Telephone: +1 734 936 4934

Fax: +1 734 763 7802

Email: davidzop@med.umich.edu

Word count: 2998

Financial disclosures

BC was funded through the MICHR TL1 Grant Number TL1TR002242 during this work. The University of Michigan SoD mCT core in which microCT was conducted was funded in part by NIH/NCRR S10RR026475-01.

Conflict of interest

BC, AC, SC, ZN, and IL have no conflicts of interest to disclose. SH is a co-founder and shareholder in Tissue Regeneration Systems Inc. SH and DZ are co-inventors on a patent entitled "Ear tissue implant for auricular tissue reconstruction." DZ is a founder in the start-up MakeMedical which utilizes the technology listed in this paper and was formed to commercialize intellectual property related to 3D-printing, but research was not funded by the company.

Abstract

Objectives

To analyze the use of highly translatable 3D printed auricular scaffolds with and without novel cartilage tissue inserts in a rodent model.

Methods

This prospective study assessed a single stage 3D-printed auricular bioscaffold with or without porcine cartilage tissue inserts in an athymic rodent model. DICOM computed tomography (CT) images of a human auricle were segmented to create an external anatomic envelope filled with orthogonally interconnected spherical pores. Scaffolds with and without tissue inset sites were 3D printed by laser sintering bioresorbable polycaprolactone (PCL) then implanted subcutaneously in five rats for each group.

Results

Ten athymic rats were studied to a goal of 24 weeks post-operatively. Precise anatomic similarity and scaffold integrity were maintained in both scaffold conditions throughout experimentation with grossly visible tissue ingrowth and angiogenesis upon explantation. Cartilage-seeded scaffolds had relatively lower rates of non-surgical site complications compared to unseeded scaffolds with relatively increased surgical site ulceration, though neither met statistical significance. Histology revealed robust soft tissue infiltration and vascularization in both seeded

and unseeded scaffolds, and demonstrated impressive maintenance of viable cartilage in cartilage-seeded scaffolds. Radiology confirmed soft tissue infiltration in all scaffolds and biomechanical modeling suggested amelioration of stress in scaffolds implanted with cartilage.

Conclusion

A hybrid approach incorporating cartilage insets into 3D-printed bioscaffolds suggests enhanced clinical and histological outcomes. These data demonstrate the potential to integrate Point of Care tissue engineering techniques into 3D-printing to generate alternatives to current reconstructive surgery techniques and avoid the demands of traditional tissue engineering.

Keywords: 3D-printing, auricular reconstruction, tissue engineering

Level of evidence: N/A (animal model)

Introduction

Auricular reconstruction is a complex and technically challenging endeavor. The most common repair technique involves the creation and implantation of an autologous construct fashioned by hand from costal cartilage, generally yielding acceptable aesthetic outcomes with a durable and compatible implant.[1,2] However, the process is demanding given the intricacy of repair, significant psychosocial sequelae, and potential complications including pneumothorax, infection, exposure of the implant, and scarring. While porous polyethylene (PPE) implants (e.g. Medpor) can provide good aesthetic outcomes, studies report higher complications including extrusion and infection when compared to rib reconstruction.[3,4]

3D printing may lessen the technical complexity of autologous implants and produce high-fidelity, biocompatible constructs similar to native tissues using tissue engineering. Some challenges with tissue engineering ear cartilage to date have been framework contraction/distortion, poor long term outcomes, and high regulatory burden using complex *in vitro* methods out of the operating room.[5-8]

To address these limitations, we have developed a hybrid scaffold-based tissue engineering approach that also allows inclusion of Point of Care autologous cartilage tissue. We previously demonstrated that our auricular scaffolds promote chondrogenesis, as seeded chondrocytes induced chondrocyte proliferation *in vitro*.[9] Here, we propose using bioscaffolds to promote chondrogenesis in clinically translatable settings that do not require *in vitro* culture, a

novel method that would have low regulatory burden, ease of performance, and capability to execute in lower resource setting, such as global outreach initiatives.

Methods

In vivo models

Scaffold development

To produce the unseeded scaffold, an external anatomic envelope was derived from computed tomography imaging of a 10-year-old male and 3D-printed in bioresorbable polycaprolactone (PCL) with orthogonally interconnected spherical pores with a mean pore diameter of 2mm.[9,10] For cartilage-seeded scaffolds, scaffolds were printed with five 2.7 mm diameter tissue inset wells at areas previously determined using nonlinear finite element analysis (FEA) to experience high effective strain leading to ulceration. All scaffolds were sterilized with ethylene oxide prior to experimentation as in prior clinical 3D printing work.[11]

Unseeded scaffold implantation

All animal surgery protocols were approved by the Institutional Animal Care and Use Committee (IACUC) at the University of Michigan (PRO00009569). Unseeded scaffolds were implanted into a subcutaneous pocket within the dorsum of five athymic rats (hereafter referred to as control group rats #1-5). Ketoprofen was administered during surgery to prevent post-operative inflammation. Incisions were closed with a subcuticular absorbable suture and covered

with cyanoacrylate tissue adhesive (3M, St. Paul, MN). Following surgery, rats were given E-collars and had their nails trimmed regularly to prevent aggressive grooming and self-induced damage to the skin over the scaffolds.

Cartilage-seeded scaffold implantation

Porcine auricles were procured approximately 16 hours prior to operating, prepared with chlorhexidine and betadine administration, then briefly kept at 2°C. The day of operation, cartilage was dissected out from skin under sterile conditions leaving the overlying perichondrium. 3.5 mm punch biopsies were procured and rinsed in sterile PBS with 250 U/ml Bacitracin and 2.50 µg/ml amphotericin B. Punch biopsies were inserted into each of the five predetermined tissue inset wells in the scaffold so that the tissue was slightly convex from the surface of the scaffold. Scaffolds were then implanted into the dorsum of five athymic rats (hereafter referred to as rats hybrid group #6-10) with peri-operative administration of ketoprofen. Rats were treated with one dose of cefazolin at 25 mg/kg approximately four hours prior to scaffold implantation and amoxicillin/clavulanic acid at 25 mg/kg twice a day for 10 days following implantation.

Clinical evaluation

Rats were subject to a weekly photodocumentation protocol with measurement of the length, width, and height of their scaffolds. They were assessed twice weekly for scaffold extrusion, site

infection, scaffold exposure/fracture, hematoma/seroma, or ulceration, with calculation of cross-sectional area of ulcers if present. Ulcers were classified according to the following system: a) "rat-induced" if markings suggested self-induced injuries including scratch marks or bite marks, b) "scaffold-induced" if ulceration was present overlying the scaffold but distinct from the suture line, c) "non-surgical site", to include rat-induced or scaffold-induced injury outside the suture site, and d) "surgical site" if ulceration was present at the suture site. Rats were sacrificed at 24 weeks with explantation of scaffolds unless otherwise stated. A two-tailed *t*-test assuming equal variances was conducted between unseeded and cartilage-seeded scaffolds comparing the maximum cross-sectional areas for each ulcer classification, with $P<0.05$ considered statistically significant.

Histological evaluation

Following explantation, three random samples of scaffold immediately surrounding punch biopsy insertion sites per rat were fixed in 4% formalin for 24 hours, embedded in paraffin, and processed using standard histologic procedures with a slice thickness of 10 μm. They were stained with hematoxylin and eosin (H&E) and Safranin O for cartilage growth assessment. Anti-pig Ki67 antibody (Neuromics, Edina, MN) was used to assess cellular proliferation in transplanted pig cartilage, and anti-rat Ki67 (BD Pharmingen, San Diego, CA) for the surrounding tissue. Cleaved caspase 3 (Cell Signaling Technology, Danvers, MA) was applied for evaluation of cellular death in both pig and rat-related tissue. To assess vascularization, H&E

slides were de-identified from their cohort (control vs. hybrid) and had four random images taken at 20x magnification (n = 12 per rat). Each image was assessed for number of vessels and the percent cross-sectional area of all blood vessels compared to overall image size (631 μm by 494 μm), where vasculature was defined by the presence of three distinct tunics (intima, media, and adventitia) with or without blood cells visible within the lumen of the vessel. Data was linked backed to the respective cohort and unpaired two-tailed t-tests assuming equal variances were conducted comparing number of vessels, average cumulative percent vessel area, and average percent vessel area per vessel, with $P<0.05$ considered statistically significant.

Radiological evaluation

Following explantation, random samples of scaffold immediately surrounding punch biopsy insertion sites were placed in a 19 mm diameter specimen holder and scanned using a microCT system (μCT100 Scanco Medical, Bassersdorf, Switzerland) with the following settings: voxel size 12 μm, 55 kVp, 109 μA, 0.5 mm AL filter, and integration time 500 ms. Scans were processed using Materialise Mimics (Leuven, Belgium) to form 3-dimensional (3D) pictures.

Biomechanical evaluation

Nonlinear FEA of scaffolds was performed using FEBio[12], modeling skin[13] and auricular cartilage[14] as nonlinear elastic materials undergoing large deformation with frictonless sliding contact conditions assumed between skin and ear scaffolds with and without biopsies.

Results

Clinical outcomes

Of rats with unseeded scaffolds, rats 2, 3, 4, and 5 made the target 24 week target date. Rat #1 was sacrificed at 19 weeks after presenting with an enlarging skin rash and over 20% weight loss despite administration of empiric antibiotics and diet pills. Cultures yielded numerous *Streptococcus sciuri* and *Enterococcus faecalis* with varying susceptibilities, suggesting complicated wound infection. Of rats with cartilage-seeded scaffolds, rats #6, 9, and 10 made the 24 week target date. Rats #7 and 8 were sacrificed at 22 weeks because of worsening surgical site ulceration.

The progression of tissue overlaying the implants with time was monitored in control (Figure 1A-C) and hybrid groups (Figure 1D-F). The average length, width, and height of scaffolds from both groups at 24 weeks was 62.6 +/- 0.55 mm, 42.8 +/- 0.45 mm, and 20.0 +/- 0.00 mm respectively, indicating that the size of the bioscaffold was stable *in vivo*. By visual comparison with original scaffolds there was no distortion of auricular subunit landmarks (superior and inferior crus of the antihelix, stem of the antihelix, triangular fossa, scaphoid fossa, conchal bowl, tragus, antitragus, intertragic notch).

Different ulceration types predominated across the groups. In the control group, 80% (4/5) had rat-induced ulceration (Figure 1G). Scaffold-induced ulcerations (80% of cases) (Figure 1H), non-surgical site ulcerations (80% of cases), and surgical site ulcerations (80% of

cases) (Figure 1I) were observed at high rates in the control group. However, the hybrid group only presented with rat-induced ulceration in 40% (2/5) of the cases. The formation of scaffold-induced ulceration (20% (1/5)) and non-surgical site ulceration was also lower (40% (2/5)) while the presence of surgical site ulceration (80% (4/5)) remained equal compared to control.

Next, we analyzed the temporal progression of cross-sectional areas for each ulceration classification. The majority of rat-induced ulcers in both control and hybrid group appeared *and regressed* within two to nine weeks with minimal wound care (Figure 1J-L). Interestingly, though there was a progressive worsening of surgical site ulcerations in 80% of the animals from both groups, we observed a smaller incidence and severity of scaffold-induced ulcers in the hybrid group compared to control. Meanwhile, different patterns of non-surgical site ulcerations were found between groups, as scaffold-induced ulcerations were predominantly seen in the control group while the hybrid group had more rat-induced ulcerations (Figure 2A). When averaging the cross-sectional ulcerations over the 2 groups (Figure 2B), we observed that the control group demonstrated more rat-induced and scaffold-induced ulcerations compared to the hybrid group, albeit not in a statistically significant fashion. In contrast, ulcerations in the hybrid group were more frequently observed at the surgical sites.

Histological outcomes

We evaluated the histology and cellular behavior of unseeded and seeded scaffolds via hematoxylin-eosin (H&E), Safranin O and Ki67/caspase 3 staining. In the control group, soft

tissue infiltration into the periphery of the pores (arrow) was observed with moderate vascularization (asterisk) (Figures 3A-C). However, no cartilage (red) was present as outlined by Safranin O staining (Figures 3D-F); we attribute scant positivity for Safranin O to staining of hair follicles.[15] H&E histology did not show concern for inflammatory infiltrates or signs of infection. In the hybrid group, we also observed robust soft tissue infiltration into the pore (Figures 3G-I, arrow) with moderate vascularization and viable perichondrium overlaying the cartilage (bracketed). Critically, we also saw maintenance of viable cartilage (red) within the transplanted punch biopsies (Figures 3J-L). Immunohistochemistry revealed proliferating pig cells in rat skin overlying the scaffold, as seen in hair follicles, and at the edge of the skin (Figure 3M/N) without porcine Ki67 antibody positivity outside of the punch biopsy. Interestingly, histology of porcine cartilage seeded in scaffold at 24 weeks also demonstrated actively proliferating cells without major cell death (Figure 3M-O).

Vascularization and blood vessel ingrowth was robust in both unseeded and hybrid seeded scaffolds. Comparable numbers of vessels per image were found on average between control and hybrid groups (6.19 vs. 6.25, $P = 0.96$, Figure 4A). Significantly larger cumulative percent vessel areas were found in the control rats vs. hybrid rats (3.18% vs. 1.87%, $P < 0.05$) but no statistical significance was found after standardizing for vessel number (0.91%/vessel vs. 0.61%/vessel, $P = 0.07$, Figure 4B).

Radiological outcomes

Lastly, we performed micro-CT on porcine cartilage punch biopsies implanted into the scaffold (Figure 5A, cartilaginous positions circled and correlated to explanted ear). Finite element analysis (FEA) models with and without biopsies (Figure 5B/C) demonstrate amelioration of strain between ear scaffolds and skin. As expected, 3D-model constructed microCT imaging of hybrid scaffolds at the time of explantation demonstrated infiltration of soft tissue into the pores (Figures 5D/E).

Discussion

Several meaningful findings resulted from this study. First, implantation of biocompatible 3D-printed PCL scaffolds seeded with cartilaginous tissue was magnitudes less technically demanding than traditional autologous microtia reconstruction, more time-efficient, and ultimately capable of sustaining viable cartilage. Grossly, 3D-printed auricles with and without cartilage inserts appeared structurally similar to human ears and all scaffold measurements remained consistent. That no significant retraction or degradation of scaffolds was observed within the period of experimentation suggests resistance to myocontractile wound healing forces and sustained longitudinal feasibility of such implants. Moreover, at the time of implantation, biopsies were intentionally larger than inset sites to allow securement through slight compression. Although inconspicuous in most cases, they were clearly visible in multiple scaffolds and found to be consistently intact on explantation without displacement; one punch biopsy may be seen prominently at the mid-stem of the helix in Figure 1F, for instance.

Critically, vascularization was identified by H&E staining in both unseeded and seeded scaffolds, implying that non-autologous tissue implants do not inhibit vessel formation within the timeframe of our experimentation. Although statistically greater cumulative percent vessel area was found in unseeded vs. seeded scaffolds, comparable vessel number between the two cohorts and the difference in percent area was rendered not statistically significant on standardization by vessel number. These differences may be explained in multiple ways. Quantification of angiogenesis has inherent challenges based on how histology captures the blood vessels. We attempted to mitigate this by taking multiple samples per slide and multiple slides per position but acknowledge that our measurement may be inaccurate and/or underestimated based on scoring from the H&E staining. Finally, although statistical differences were observed, they still arose only in the context of two cohorts of five rats each, and this study was not specifically powered to detect differences between the groups. Overall, vascularization was detected both grossly and histologically in each of the seeded and unseeded scaffold, and we believe this level of vascularization is likely to improve overlying soft tissue quality when compared to the high density nature of PPE.[16,17]

Regarding chondrogenesis, viable cartilage was confirmed by Safranin O in punch biopsy sites along with Safranin O positive tissue on the periphery of the pores in the seeded scaffold. In addition to cartilage, viable perichondrium was observed on histology. Studies have previously established that chondrocyte progenitor cells are found within the perichondrium of adult auricular tissue.[18] With demonstration of perichondrial survival, we can envision co-culturing

perichondrium with multipotent cell populations – for example adipose derived stem cells – to evaluate its impact on differentiation and chondrogenic potential. Subjectively, we noted that the soft tissue overlying the scaffolds was thicker in tissue-seeded vs. unseeded scaffolds, as seen in Figures 3A compared to figure 3G. However, additional analysis is required to confirm these differences.

Distinct patterns of ulceration were noted between the unseeded and cartilage-seeded scaffolds. First, healing of rat-induced ulceration was seen across both conditions, consistent with the discovery of vascularization. Second, smaller rates of scaffold-induced ulceration approaching statistical significance were seen in the cartilage-seeded scaffolds. This suggests that inclusion of the cartilage tissue biopsies intended to offset the interface between overlying soft tissue and that rigid scaffold was successful in ameliorating frictional strains, consistent with our FEA models in Figures 5B/5C. Finally, it appears that greater cross-sectional area of surgical site ulceration was present with the cartilage-seeded scaffolds compared to unseeded scaffolds, although this difference was not statistically significant. We hypothesize that even a slight increase in the volume of the offset may add small but meaningful amount of stress on the wound closure and that our closure technique utilizing a subcutaneous running Monocryl – which normally performs well in humans – might be more challenging in the post-operative care of animals. In the future, we could potentially address this complication by decreasing projection of the cartilage from the scaffold and balancing tension with a contralateral otoplasty.

There exist several key points that merit discussion. The first is that no statistically significant difference was observed between cartilage-seeded and unseeded scaffolds in any category of ulceration. This is likely due to limited sample size and the methods by which measurements were obtained. In the rat-induced ulceration category for example, it is possible that there are multiple occult signs that were not accounted for, including rubbing on the sides of the cage with subsequent scaffold displacement. Beyond statistical analysis, the exact relationship between Safranin O positive tissue and chondrogenesis could not be determined with regard to the originating tissue. Specifically, one can imagine scenarios in which porcine cartilage induced a microenvironment whereby native circulating mesenchymal stem cells seeded around the punch biopsy were induced towards the chondrocytic lineage, or alternatively where porcine mesenchymal stem cells were transplanted along with the auricular tissue and contributed to peripheral chondrogenesis. As such, additional immunohistochemistry will be essential towards clarifying whether chondrocytes are present beyond the limits of the cartilage punch biopsy and from which tissue they arise.

While the utility of 3D-printing has grown dramatically in medicine at large, cartilage engineering in particular has benefited from its developments. Successful cartilage growth was shown by Cohen in athymic rat and mouse models with implantation of bioscaffolds seeded with *in vitro* cultured chondrocytes and mesenchymal stem cells.[19] Kim *et al.* seeded 3D-printed auricular scaffolds with tonsil-derived mesenchymal stem cells, then implanted those scaffolds into mouse models with demonstration of collagen and vascularization after 12 weeks.[20]

Additionally, Zhou *et al.* isolated auricular cartilage-derived chondrocytes from microtia patients, cultured them in a bioscaffold for four months, and implanted them back into the patients to observe successful outcomes after 2.5 years.[21] All these concepts are promising, but unfortunately require a significant *in vitro* component with extensive culturing time that may not be readily translatable in all institutions. Furthermore, these cells cultured outside the OR combined with scaffolds are a class III combination product that face significant regulatory expense and time to achieve FDA approval for clinical use including performing phase I and phase II clinical trials. Exclusively *in vivo* approaches have been tried too, with chondrogenesis obtained in bioscaffolds seeded with autologous diced cartilage and platelet-rich plasma in rabbit models.[22] However, even this required some processing after collecting tissue/serum, and a cystic-like reaction was induced around the scaffold at explantation at four months, indicating that improvements are still warranted. In comparison to these methods, our work has fewer technical requirements in combining point of care tissue engineering with 3D printing and do not require advanced technology, e.g. bioprinting with cells plus materials. As a result, this work has great potential in global outreach, where organizations and facilities may not have the same capacities as those within the U.S.

In summary, we show a promising new technique for auricular reconstruction that is reproducible, relatively less technically complex, and most importantly, readily clinically translatable as it eliminates *in vitro* requirements and accompanying regulatory burden. One can imagine a situation in which a bioscaffold is customized and printed for a patient, seeded with

autologous tissue, and implanted within the same day. With further iterations, we hope to expand this project to additional animal models, use autologous tissues, extend the period of observation after implantation, and ultimately translate towards human patients.

Acknowledgements

We would like to thank the Extracorporeal Circulation Research Laboratory and Dr. Hsun-Liang Chan of the Department of Periodontics and Oral Medicine for their donation of pig tissue, and Drs. Patrick Lester and Anna Skorupski of the Animal Care and Use Program for their assistance in animal care.

References

1. Cubitt JJ, Chang LY, Liang D, Vandervord J, Marucci DD. Auricular reconstruction. *J Paediatr Child Health.* 2019;55(5):512-517.
2. Olshinka A, Louis M, Truong TA. Autologous Ear Reconstruction. *Semin Plast Surg.* 2017;31(3):146-151.
3. Cenzi R, Farina A, Zuccarino L, Carinci F. Clinical outcome of 285 Medpor grafts used for craniofacial reconstruction. *J Craniofac Surg.* 2005;16(4):526-530.
4. Constantine KK, Gilmore J, Lee K, Leach J, Jr. Comparison of microtia reconstruction outcomes using rib cartilage vs porous polyethylene implant. *JAMA Facial Plast Surg.* 2014;16(4):240-244.
5. Reiffel AJ, Kafka C, Hernandez KA, et al. High-fidelity tissue engineering of patient-specific auricles for reconstruction of pediatric microtia and other auricular deformities. *PLoS One.* 2013;8(2):e56506.
6. Bichara DA, O'Sullivan NA, Pomerantseva I, et al. The tissue-engineered auricle: past, present, and future. *Tissue Eng Part B Rev.* 2012;18(1):51-61.
7. Tack P, Victor J, Gemmel P, Annemans L. 3D-printing techniques in a medical setting: a systematic literature review. *Biomed Eng Online.* 2016;15(1):115.
8. Jung CS, Kim BK, Lee J, Min BH, Park SH. Development of printable natural cartilage matrix bioink for 3D printing of irregular tissue shape. *Tissue Eng Regen Med.* 2018;15(2):155-162.
9. Zopf DA, Flanagan CL, Mitsak AG, Brennan JR, Hollister SJ. Pore architecture effects on chondrogenic potential of patient-specific 3-dimensionally printed porous tissue bioscaffolds for auricular tissue engineering. *Int J Pediatr Otorhinolaryngol.* 2018;114:170-174.
10. Zopf DA, Mitsak AG, Flanagan CL, Wheeler M, Green GE, Holliser SJ. Computer aided-designed, 3-dimensionally printed porous tissue bioscaffolds for craniofacial soft tissue reconstruction. *Otolaryngol Head Neck Surg*. 2015;152(1):57-62.
11. Zopf DA, Hollister SJ, Nelson ME, Ohye ERG, Green GE. Bioresporbable airway spint created with a three-dimensional printer. *N Engl J Med*. 2013;368(21):2043-2045.
12. Maas SA, Ellis BJ, Ateshian GA, Weiss JA. FEBio: finite elements for biomechanics. *J Biomech Eng.* 2012;134:011005.
13. Shergold OA, Fleck NA. Experimental investigation into the deep penetration of soft solids by sharp and blunt punches, with application to the piercing of skin. *J Biomech Eng.* 2005;127:838-848.
14. Zopf DA, Flanagan CL, Nasser HB, et al. Biomechanical evaluation of human and porcine auricular cartilage. *Laryngoscope.* 2015;125:E262-268.
15. Safranin. Conduct Sciences. https://conductscience.com/lab/safranin/, accessed 4/22/2020.86(5):445-457.

16. Stephan S and Reinisch J. Auricular reconstruction using porous polyethylene implant technique. *Facial Plast Surg Clinics of North Am*. 2018;26(1):69-85.
17. Schroeder MJ and Lloyd MS. Tissue engineering strategies for auricular reconstruction. *J Craniofac Surg*. 2017;28(8):2007-2011.
18. Togo T, Utani A, Naitoh M, et al. Identification of cartilage progenitor cells in the adult ear perichondrium: utilization for cartilage reconstruction. *Lab Invest*. 2006;86(5):445-457.
19. Cohen BP, Bernstein JL, Morrison KA, Spector JA, Bonassar LJ. Tissue engineering the human auricle by auricular chondrocyte-mesenchymal stem cell co-implantation. *PLoS One.* 2018;13(10):e0202356.
20. Kim HY, Jung SY, Lee SJ, Lee HJ, Truong MD, Kim HS. Fabrication and characterization of 3D-printed elastic auricular scaffolds: A pilot study. *Laryngoscope.* 2019;129(2):351-357.
21. Zhou G, Jiang H, Yin Z, et al. In Vitro regeneration of patient-specific ear-shaped cartilage and its first clinical application for auricular reconstruction. *EBioMedicine.* 2018;28:287-302.
22. Liao J, Chen Y, Chen J, et al. Auricle shaping using 3D printing and autologous diced cartilage. *Laryngoscope.* 2019;129(11):2467-2474.

Figure titles

Figure 1. Representation of scaffolds and/or ulcerations over time *in vivo*.

Figure 2. Trended mitigation of a majority of soft tissue ulceration mechanisms by hybrid approach.

Figure 3. Soft tissue integration, angiogenesis, and maintenance of viable cartilage in the hybrid approach.

Figure 4. Quantitative analysis of vascularization in control (C) and hybrid (H) rat scaffolds.

Figure 5. Biomechanical modeling and microCT imaging of cartilage-seeded bioscaffolds.

Figure legends

Figure 1. Photodocumentation of a representative rat with unseeded scaffold (A) immediately following implantation, (B) 12 weeks after implantation, and (C) 24 weeks post-implantation. Photodocumentation of a representative rat with hybrid cartilage-seeded bioscaffold (D) immediately after implantation, (E) 12 weeks, and (F) 24 weeks after implantation. Representative examples of (G) rat-induced, (H) scaffold-induced, and (I) surgical site ulceration. Progression of non-surgical and surgical site ulceration of representative rat with cartilage-seeded bioscaffold at (J) 13, (K) 15, and (L) 17 weeks after implantation, with demonstration of healing in lateral wounds.

Figure 2. (A) Graphs representing cross-sectional area of ulcerations in control and hybrid groups according to type of ulceration (rat-induced, scaffold-induced, non-surgical site, or surgical site) and average maximum cross-sectional area. Error bars represent standard error. (B) Average and standard error (SEM) of ulceration cross-sectional area in mm^2 in unseeded and cartilage-seeded scaffolds. *P*-value determined from two-tailed *t*-test assuming equal variances.

Figure 3. Unseeded scaffold histology under H&E staining (A-C) and Safranin O staining (D-F). Cartilage-seeded scaffold histology with H&E staining (G-I) and Safranin O staining at (J-L). Scale bar represents 1000 μm in Fig A, D, G, and J; 200 μm in Fig B, E, H, and K; and 100 μm in Fig C, F, and I. Arrows point to soft tissue ingrowth. Asterisk represents vascularization. Brackets encompass viable perichondrium. Immunohistochemical staining for Ki67 (green), caspase 3 (red), and Dapi (grey) at different localizations in and/or surrounding the cartilage-seeded bioscaffold (M-O); scale bar represents 100 μm.

Figure 4. (A) Average vessel number per image (311,714 μm^2). (B) Cumulative percent vessel area and percent vessel area normalized by vessel number per image. C represents the control group, H represents the hybrid group.

Figure 5. (A) A representative scaffold seeded with porcine auricular cartilage biopsies (circled) mapped to a hybrid scaffold. (B) FEA model of PCL scaffolds (green) without biopsy but containing insert holes, and resulting strain in idealized skin pulled over ear scaffold. (C) FEA model of PCL scaffolds with biopsy, and resulting in reduced high strain areas in idealized skin pulled over ear scaffold. (D) MicroCT imaging of a cartilage-seeded scaffold with tissue

infiltration circled. (E) 3D rendered model of a cartilage punch biopsy after explantation of the scaffold.

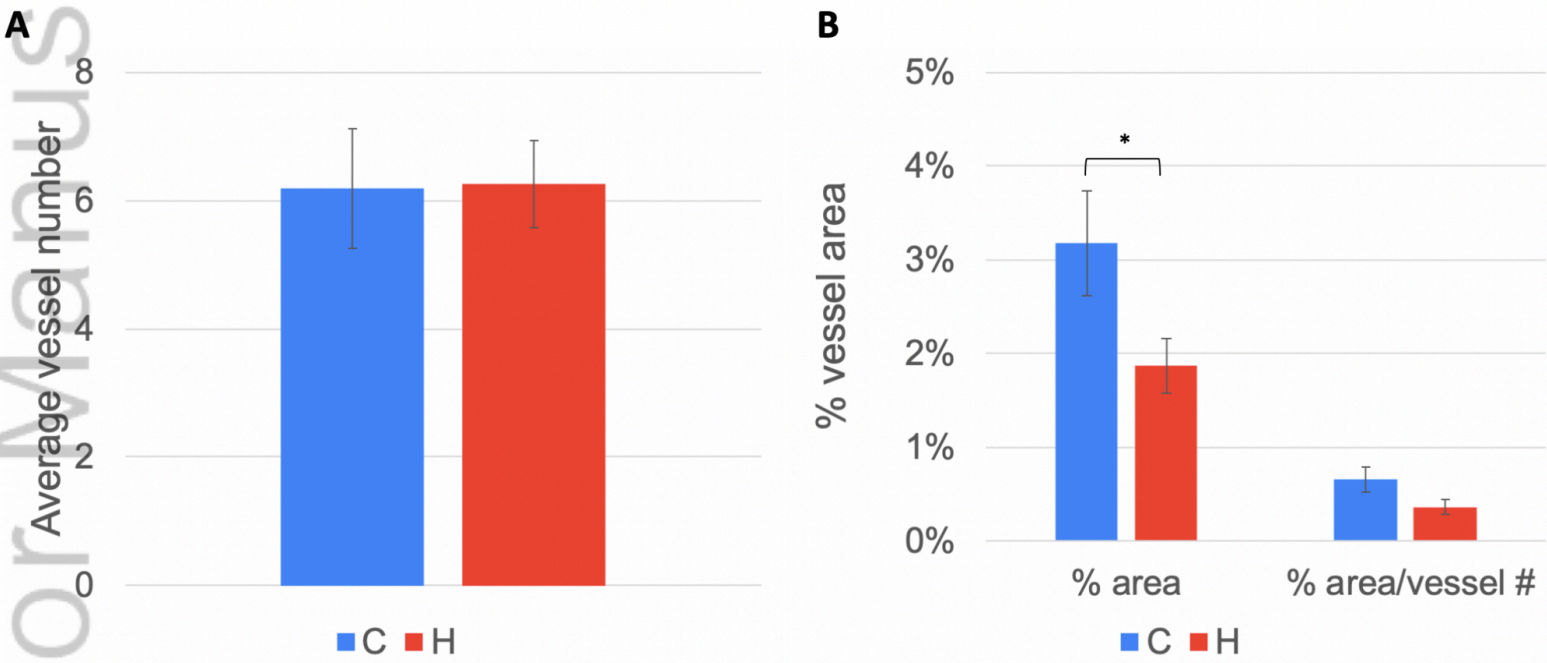

LARY_29114_3.13.20 Figure 4.png

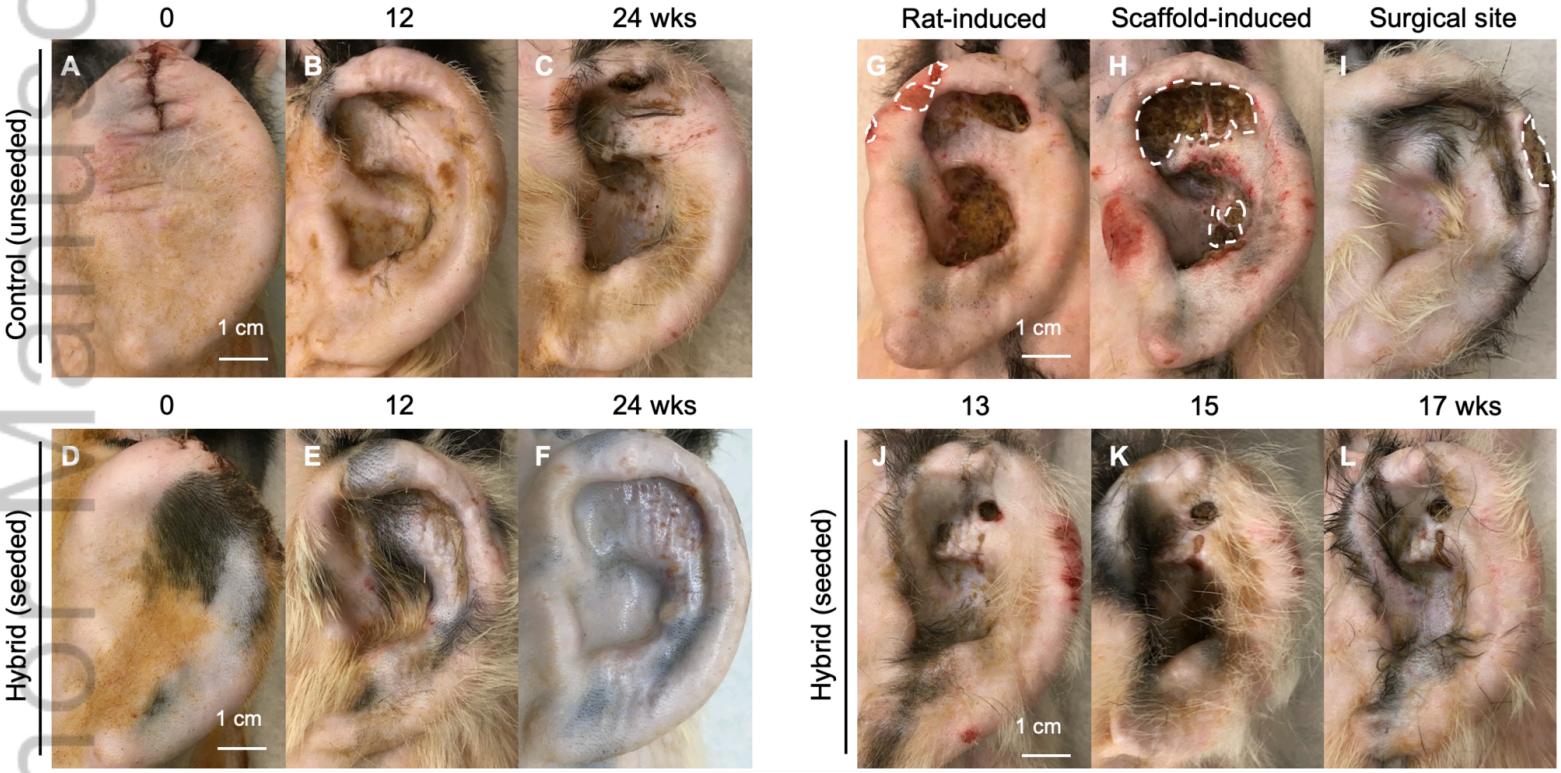

LARY_29114_4.6.20 Figure 1.png

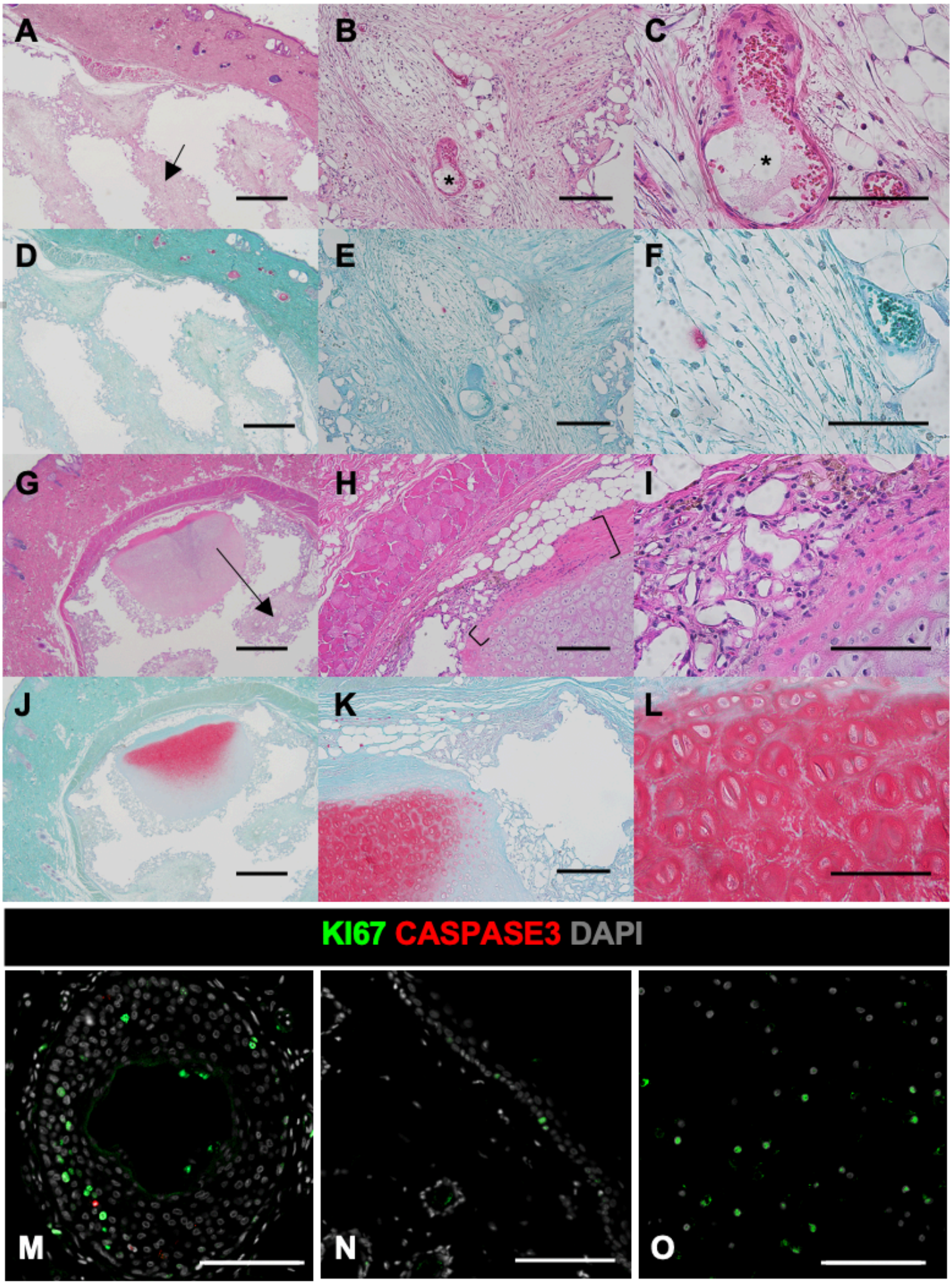

A

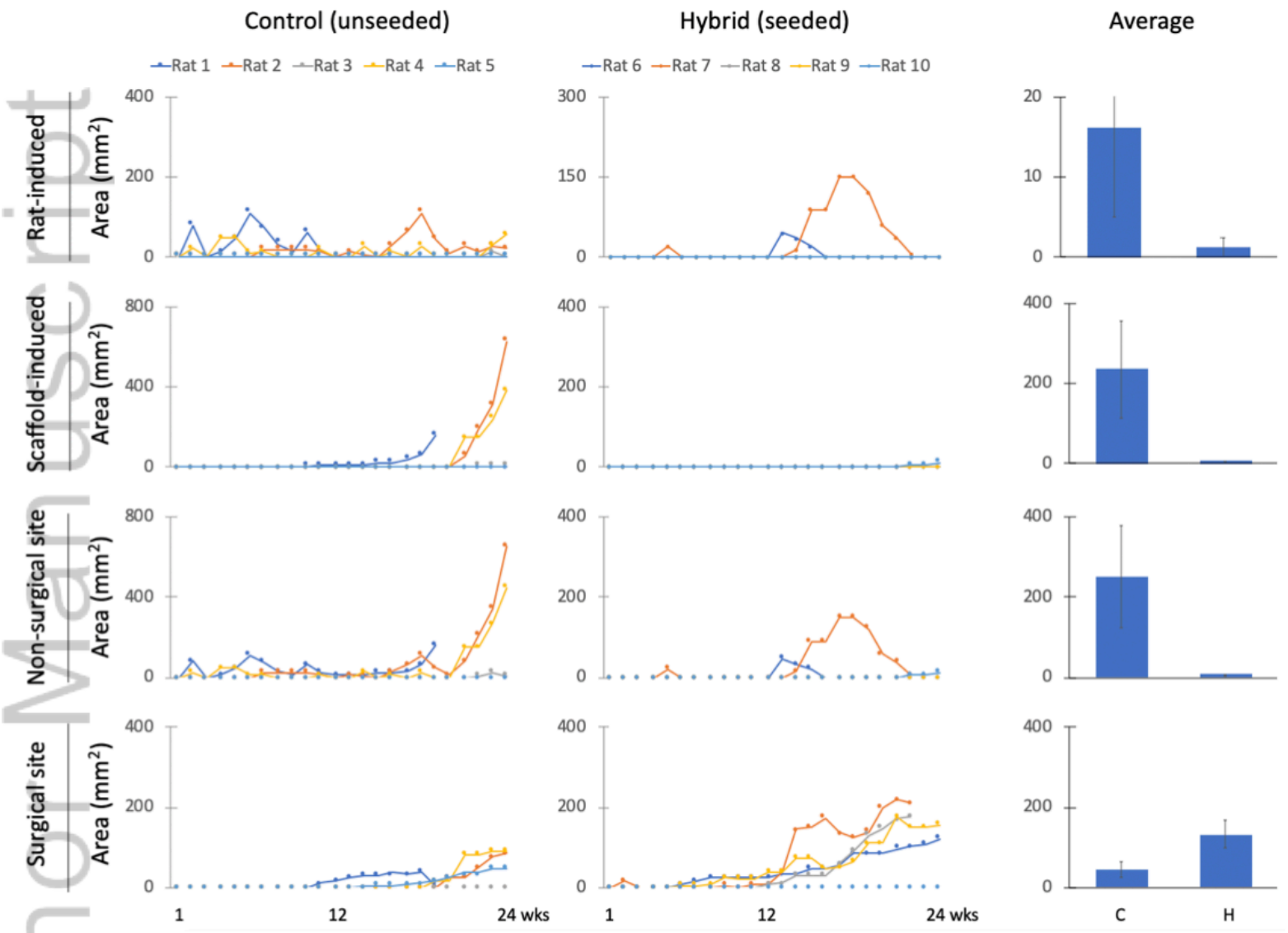

B

Ulceration	Control group		Hybrid group		*P*-value
	Average	SEM	Average	SEM	
Rat-induced	135.0	80.4	3.2	2.1	0.140
Scaffold-induced	236.4	120.3	2.0	2.0	0.087
Non-surgical site	371.4	175.2	5.2	3.9	0.070
Surgical site	52.0	16.4	138.0	37.8	0.071

LARY_29114_5.23.20 Figure 2.png